Mimicking Boyer's Casimir repulsion with a nanowire material

Stanislav I. Maslovski* and Mário G. Silveirinha
Departamento de Engenharia Electrotécnica, Instituto de Telecomunicações, Universidade de Coimbra
Pólo II, P-3030-290 Coimbra, Portugal
(Received 19 October 2010; published 24 February 2011)

It is shown that the electromagnetic Casimir force acting on a conducting body (e.g., a realistic metallic piston) sliding in a background formed by cut silver nanorods (with the body perforated by the nanorods) is repulsive at distances larger than the separation of the nanorods, even if the host material of the nanorods is air. It is demonstrated that the physical origin of this effect is in essence related to Boyer's prediction that magnetic and conducting walls repel each other. Indeed, we show that from the point of view of an observer inside the nanowire structure, the interface formed by severing the nanowires mimics accurately the behavior of a magnetic wall for *P*-polarized waves. In contrast to other piston configurations reported in the literature, the Casimir interaction in the nanowire background is an ultralong-range force that decays with the distance to the nearby interface as $1/a^2$.

DOI: 10.1103/PhysRevA.83.022508 PACS number(s): 31.30.jh, 12.20.−m, 42.50.Lc, 42.70.Qs

I. INTRODUCTION

The Casimir-Lifshitz forces [1–3] and especially the so-called Casimir repulsion [4–10] or "quantum levitation" [11–14] phenomena in structures of different geometries have been topics of continuous research for many decades. In simple geometries involving planar dielectric or metallic plates in a vacuum, the electromagnetic Casimir force is always attractive, while when the plates are immersed in a dielectric fluid, one can obtain a repulsive force if the permittivities of the plates and the fluid are chosen appropriately [15]. A repulsive force may be also obtained if a conducting plate is combined with a permeable plate [4].

The geometry of interest in this paper is a variant of the so-called Casimir piston geometry [16–21]. A piston is a sliding reflecting wall placed inside a waveguide or cavity. The force acting on such a wall can be calculated provided the cavity modes on both sides of the piston are known. It can be shown that a conducting piston in a conducting cylindrical cavity always attracts to the wall at the nearest end of the cavity [17]. On the other hand, if the walls of the cavity and the piston are weakly reflecting, the force can be repulsive at certain separations [18].

Studies involving pistons in cavities of canonical geometries are, of course, of great importance and interest. However, from a rather intuitive physical consideration it can be seen that the Casimir forces acting on pistons in elongated waveguides or cavities of simply connected cross sections are always weak and short range. Indeed, consider a rectangular cavity with cross section $a \times b$ and length $L \gg a \geqslant b$. In such a waveguide, the modes have the dispersion of the form $k_z = (\omega/c)\sqrt{1-\omega_c^2/\omega^2}$ (the z axis is along the longest dimension of the cavity), where ω_c is the characteristic cutoff frequency of a waveguide mode. On the positive half of the imaginary axis, the frequency is $\omega = i\xi$, and the dispersion relation can be rewritten as $\gamma_z = (\xi/c)\sqrt{1+\omega_c^2/\xi^2}$, where $\gamma_z = -ik_z$ is the attenuation factor of a mode [we assume a time dependence of the form $\exp(-i\omega t)$]. Thus, at imaginary frequencies the attenuation factor of a mode is always greater than ω_c/c and grows with ξ. The mode with the lowest possible attenuation is the main transverse electric TE_{10} mode that has $\omega_c/c = \pi/a$. Therefore, the effective range of interactions due to virtual photons in such a waveguide is of order of a and is always limited by the cross-section size of the cavity.

The situation changes in waveguides with cross sections that are not simply connected, where there are modes with $\omega_c = 0$: the so-called transverse electromagnetic (TEM) modes. The effect of these modes in simple coaxial structures has been considered in literature but found to be negligible when compared to the effect of the other modes [22]. However, in a recent work [23] we have shown that if the number of independent TEM modes supported by a structure grows linearly with the cross-sectional area of the structure, the Casimir forces due to the TEM modes may become dominant, especially at large separations. In particular, this happens when the interacting bodies (e.g., dielectric plates) are immersed in a periodic arrangement of metallic nanorods. In simple words, the nanorods effectively channel the quantum fluctuations of the electromagnetic field to distances that are orders of magnitude larger than the transverse separation of the nanorods, boosting in this manner the Casimir force at large distances.

Some theoretical works predict that the force acting on an ideally conducting piston sliding in a cavity with ideally permeable walls is repulsive [21]. This is, of course, not surprising, because it is known since the study of Boyer that ideally permeable (perfect magnetic conductor, PMC) and ideally conducting (perfect electric conductor, PEC) plates repel in vacuum [4]. One could think that by using metamaterials or patterned surfaces it might be possible to mimic to some extent the behavior of a PMC wall in the context of the Casimir effect. However, recently it has been shown that causality and passivity severely limit the possibilities of Casimir repulsion with slabs of metal-dielectric metamaterials standing *in a vacuum* [10,24]. In simple terms, this is due to the fact that at large separations (relative to the scale of the period of a metamaterial) the sign of the Casimir force is determined

*stas@co.it.pt

by the low-frequency response, and at low frequencies all metal-dielectric composites necessarily lose their magnetic properties [25].

However, in this work we show that *in a wire medium background* (i.e., in the effective medium formed by a periodic array of parallel metallic nanorods: see Fig. 1) a boundary condition equivalent to a PMC can be realized rather easily for the TEM waves in a wide frequency range, just by severing the nanorods at the desired plane. Moreover, the lower the frequency, the better the PMC approximation becomes! Thus, it is expected that a metallic body embedded in such wire medium background will be repelled away from the interfaces where the PMC condition is mimicked.

This intriguing result can be unveiled by making a parallel between the uniaxial nanowire medium and a multiwire transmission line. Indeed, consider an open-end termination of a transmission line. At such a termination, the line current is zero and the line voltage is at maximum. This means that the reflected wave is in phase with the incident one, and the reflection coefficient is $\rho = +1$, that is, an open end of a transmission line is effectively a PMC termination for the waves propagating in the line (we neglect radiation from the open end, which can be made arbitrarily small at low frequencies). An analogous phenomenon happens in uniaxial wire media: the reflection coefficient for the TEM waves *traveling inside the wire medium* and incident on a wire medium–air interface (with the wires orthogonal to the interface) is close to $+1$ when the transverse wave number $k_t \gg \omega/c$; that is, such an interface is effectively a PMC for these waves. Thus, since at large separations the Casimir force is mainly determined by the TEM waves [23], a dielectric or conducting plate embedded in cut nanorods must effectively repel from the open ends of the nanorods at such separations. In what follows, we further develop this simple idea and demonstrate that indeed the Casimir force acting on a piston sliding in cut metallic nanorods is an ultralong-range repulsive force.

II. CASIMIR'S FORCE ON PMC AND PEC PLATES EMBEDDED IN NANOWIRES

In this section, we briefly outline some results related to the interaction of ideally conducting and ideally permeable plates in a nanowire background. In Ref. [23], we considered Casimir's force exerted on PEC plates embedded in PEC nanowires (this force is attractive; the TEM contribution to the force is given by Eq. (5) of Ref. [23]) and also generalized it to arbitrary nondispersive magnetodielectrics in PEC nanowires, with the contribution of the TEM modes given by Eq. (7) of Ref. [23] (for simplicity, the nanowires are assumed to stand in air):

$$\frac{F_{\mathrm{TEM}}}{L^2} = \frac{\hbar c\, \mathrm{Li}_2(r_1 r_2)}{4\pi a^2 b^2}, \tag{1}$$

where F_{TEM}/L^2 has the meaning of Casimir's force per unit area, a is the separation between the plates, b is the period of the nanowire lattice, $\mathrm{Li}_2(z) = \sum_{n=1}^{\infty} z^n/n^2$ is the dilogarithm function, and $r_{1,2}$ are the reflection coefficients of TEM modes at the plate surfaces.

Formula (1) reduces to Eq. (5) of Ref. [23] when $r_1 r_2 = 1$ (two PEC plates, or two PMC plates), in which case the force is attractive because $\mathrm{Li}_2(1) = \pi^2/6 > 0$ (in [23] we

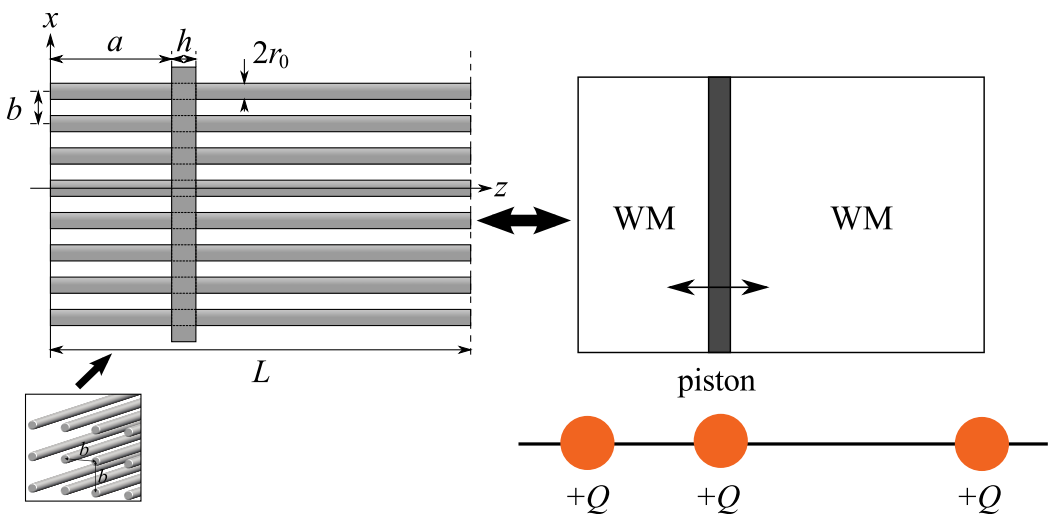

FIG. 1. (Color online) Left: A square $b \times b$ array of metallic nanorods of length L and radius r_0 with a metallic or dielectric piston of thickness h embedded in the array (side view; the three-dimensional structure is shown within the small inset). The structure is periodic and infinite in the plane orthogonal to the nanorods (in the xoy plane). We assume that the nanorods are held fixed and cannot move (e.g., the ends of nanorods may be attached to thin dielectric sheets), while the piston is perforated by the nanorods and is able to slide on them. Top right: Effective medium portrait of the structure shown at the left. The array of nanorods is represented by a continuous background material: *the wire medium* (WM). Bottom right: An electrostatic analogy of the repulsion phenomenon under study. Three equally charged beads on a stretched thread. The beads on the left and right are fixed on the thread, while the bead in the middle can slide. The equilibrium is reached when the sliding bead is at the geometrical center. Notice that if there is no thread and the relative movement of the beads is not limited, then there is no stable equilibrium.

used a convention that a positive force corresponds to attraction).

The case of $r_1 r_2 = -1$ corresponds to the generalization of Boyer's configuration [4]: an ideally conducting plate and an ideally permeable plate are embedded in the nanowire background. In this case, $\mathrm{Li}_2(r_1 r_2) = \mathrm{Li}_2(-1) = -\pi^2/12 < 0$; that is, the force is repulsive. From (1) it is also seen that this force is ultralong range, as it varies with the separation between the plates as $1/a^2$, while the repulsive force in the original configuration by Boyer has a characteristic dependence of $1/a^4$: $F_{\mathrm{v}}/L^2 = -(7\pi^2/8)(\hbar c/240a^4)$. In particular, we see that

$$\frac{F_{\mathrm{TEM}}}{F_{\mathrm{v},P}} = \frac{80}{7\pi}\frac{a^2}{b^2}, \tag{2}$$

where $F_{\mathrm{v},P} = F_{\mathrm{v}}/2$ represents the component of the force due to oscillators associated with P-polarized modes. Thus, in presence of the nanowires, the force due to P-polarized modes is boosted by the factor given by (2). For thin wires, the component of the force due to S-polarized modes is roughly the same in the two cases [23].

The enhancement of the Casimir interaction can be explained by the dramatically large density of photonic states in the nanowire background as compared to the density of states in vacuum. Indeed, the contribution of the TEM modes to the density of photonic states (per unit of volume) in the nanowire background is

$$D_{\mathrm{TEM,WM}}(\omega) = \frac{1}{(2\pi)^3}\int \delta(\omega - \omega_{\mathbf{k},\mathrm{TEM}})\, d^3\mathbf{k}. \tag{3}$$

For PEC wires, the dispersion of the TEM modes is $\omega_{\mathbf{k},\mathrm{TEM}} = c|k_z|$. Hence, assuming that the wires are arranged in a square lattice with period b, and using the fact that the TEM branch can always be assumed to be within the first Brillouin zone [23], we find that

$$D_{\mathrm{TEM,WM}}(\omega) = \frac{1}{(2\pi)^3}\int_{-\pi/b}^{+\pi/b}\int_{-\pi/b}^{+\pi/b}\int_{-\infty}^{+\infty} \times \delta(\omega - |k_z|c)\, dk_x\, dk_y\, dk_z = \frac{1}{\pi b^2 c}. \tag{4}$$

Perhaps a more intuitive way of deriving the same result is by noticing that in the volume $V = L \times L \times a$ in between the plates there are $N = L^2/b^2$ distinct nanowires and thus exactly N independent normal TEM oscillations (standing waves) at a given frequency [23]. From the dispersion relation, it follows that on the frequency axis the modes are spaced by $\Delta\omega = \pi c/a$, and therefore the density of states is $N/(V\Delta\omega) = 1/(\pi b^2 c)$.

On the other hand, the contribution of P-polarized waves to the density of photonic states in vacuum is $D_{P,fs}(\omega) = \omega^2/(2\pi^2 c^3)$. Thus, we find that

$$\frac{D_{\mathrm{TEM,WM}}(\omega)}{D_{P,fs}(\omega)} = \frac{2\pi c^2}{b^2\omega^2}. \tag{5}$$

Therefore, for long wavelengths the density of states in the nanowire material is independent of frequency and thus much larger than in free space.

The enhancement of the Casimir force readily follows from this result, because to each classical eigenmode corresponds a quantum oscillator. It is also relevant to note that the TEM modes propagate along the wires, and thus they always promote the interaction between the two plates. Curiously, it is possible to estimate the enhancement of the Casimir force using Eq. (4). In fact, roughly speaking, the oscillators that will contribute most to the Casimir force are associated with frequencies such that $\omega \lesssim \pi c/a$, being a the distance between the PEC and PMC plates. Hence, we can estimate that the enhancement of the Casimir force is roughly the ratio between the number of photonic states with frequency less than $\omega_c = \pi c/a$. This yields

$$\frac{F_{\mathrm{TEM}}}{F_{\mathrm{v},P}} \sim \frac{\int_0^{\omega_c} D_{\mathrm{TEM,WM}}(\omega)d\omega}{\int_0^{\omega_c} D_{P,fs}(\omega)d\omega} = \frac{6\pi c^2}{b^2}\frac{1}{\omega_c^2} = \frac{6a^2}{\pi b^2}, \tag{6}$$

which is of the same order of magnitude as the exact result [Eq. (2)]. It is important to mention that the increase of the density of photonic states in periodic media has been discussed before in the literature in the context of the Purcell effect and metamaterials and remarkably in the case of hyperbolic media [26,27]. In particular, in a recent work it was shown that the spontaneous emission can be enhanced when the emitter is placed near an array of nanorods [28].

In the following sections, we demonstrate that it is possible to mimic the interaction between a PEC plate and a PMC plate embedded in a nanowire background simply by severing the nanorods. As mentioned in the introduction, our aim is to show that the interface with cut nanorods is effectively a PMC for the TEM modes, and thus a metallic piston sliding in the nanorods is repelled away from such interface. We consider the effect of realistic dispersion in all the materials.

III. CASIMIR INTERACTION ENERGY FOR A SEMITRANSPARENT PISTON IN A WIRE MEDIUM BACKGROUND

The geometry of the structure under study in this work is shown in Fig. 1. It is a dense square $b \times b$ lattice of cut nanorods of radius $r_0 \ll b$. The length of the nanorods is $L \gg b$. As discussed, from the point of view of an observer *inside* the nanowire array, the interfaces $z = 0$ and $z = L$ effectively behave as magnetic walls, even if the nanowires stand in a vacuum. Thus, it is expected that if a metal-dielectric body or particle is placed inside this periodic structure, it will be repelled away from the interfaces due to the quantum fluctuations of the electromagnetic field. For simplicity of modeling, in this work we restrict the discussion to the case of a sliding wall (a piston) at distance a from the ends of the nanorods, as illustrated in Fig. 1. The piston is either a metallic or dielectric slab of thickness h perforated with the nanorods so that it can slide freely along the nanorods, while the movements in the orthogonal directions or rotations are forbidden. The structure is infinite in the transverse direction; thus, we are interested in the force per unit cross-sectional area of the piston (i.e., in the pressure).

We restrict our analysis to the case with $a \gg b$ and also $L - a - h \gg b$. In our previous work [23], it was demonstrated that under these assumptions the Casimir force can be calculated using an effective medium approach. Namely,

when homogenized, a dense lattice of metallic nanorods can be described by the following uniaxial nonlocal permittivity dyadic [29–31]:

$$\frac{\bar{\bar{\varepsilon}}(\omega,\mathbf{k})}{\varepsilon_0\varepsilon_h} = \varepsilon_t \bar{\bar{I}}_t + \left(1 - \frac{\beta_p^2}{\beta^2 + \beta_c^2 - k_z^2}\right)\hat{\mathbf{z}}\hat{\mathbf{z}}, \tag{7}$$

where $\bar{\bar{I}}_t$ is the unity dyadic in the xoy plane, k_z is the z component of the wave vector $\mathbf{k}$, ε_h is the relative permittivity (with respect to the permittivity of vacuum ε_0) of the host material where the nanorods are embedded, $\beta = \omega\sqrt{\varepsilon_0\varepsilon_h\mu_0}$ is the wave number in the host material, and ε_t is the normalized effective transverse permittivity. For thin metallic nanorods, $\varepsilon_t \approx 1 + (2\pi r_0^2/b^2)(\varepsilon_r - \varepsilon_h)/(\varepsilon_r + \varepsilon_h)$, where ε_r is the relative complex permittivity of metal; in our case, when $r_0 \ll b$ one may use the approximation $\varepsilon_t \approx 1$. The remaining parameters in Eq. (7) are $(\beta_p b)^2 = 2\pi/[\log(b/2\pi r_0) + 0.5275]$ and $\beta_c^2 = -\beta_p^2(b^2/\pi r_0^2)[\varepsilon_h/(\varepsilon_r - \varepsilon_h)]$ (here and in what follows $\log(x)$ denotes the natural logarithm).

It can be shown (e.g., with the argument principle [24,32,33]) that, at zero absolute temperature, the regular part of the zero-point energy per unity of the cross-sectional area of the structure under study can be written as

$$\delta\mathcal{E}_c(a) = \frac{\hbar}{2\pi^3}\int_0^{\pi/b}\int_0^{\pi/b}\int_0^{\infty} \log D(a,i\xi,k_x,k_y)\, d\xi\, dk_x\, dk_y, \tag{8}$$

where $D(a,\omega,k_x,k_y)$ determines the characteristic equation of the normal modes: the solutions of $D(a,\omega,k_x,k_y) = 0$ yield the resonant frequencies of the normal Bloch modes characterized by a given pair of transverse wave numbers (k_x,k_y). Notice that we only consider values of (k_x,k_y) in the first quadrant of the Brillouin zone, because due to the symmetry of the structure the contribution from the first quadrant is one-fourth of the contribution of the entire Brillouin zone.

In order that Eq. (8) represents the interaction energy, the function $D(a,\omega,k_x,k_y)$ must be such that (i) the integral in Eq. (8) exists and is finite at finite separations $0 < a < L - h$, which implies that $D(a,i\xi,k_x,k_y) \to 1$ when $\xi \to \infty$; (ii) $\delta\mathcal{E}(a) \to 0$ when both $a \to \infty$ and $L - a \to \infty$; (iii) the poles of $D(a,\omega,k_x,k_y)$ in the variable ω must be independent of a, that is, of the position of the piston. The last requirement comes from the derivation of Eq. (8) as a path integral in the complex plane ω.

The characteristic equation of the whole structure can be obtained as follows (here and in what follows, we assume $r_0 \ll b$, so that $\varepsilon_t \approx 1$). Inserting Eq. (7) into the source-free Maxwell's equations and considering the plane-wave solutions with fixed $\mathbf{k}_t = k_x\hat{\mathbf{x}} + k_y\hat{\mathbf{y}}$, one obtains the dispersion equation for the eigenwaves in a slab of nanorods. The solutions are [29]

$$k_z = \pm\sqrt{\beta^2 - k_t^2}, \tag{9}$$

for the S-polarized eigenwaves (with $E_z = 0$), and

$$k_z = \pm\Big[\beta^2 - \tfrac{1}{2}\Big(\beta_p^2 + k_t^2 - \beta_c^2 \pm \sqrt{\left(\beta_p^2 + k_t^2 - \beta_c^2\right)^2 + 4\beta_c^2 k_t^2}\Big)\Big]^{1/2}, \tag{10}$$

for the P-polarized eigenwaves (with $H_z = 0$). Notice that due to the spatial dispersion effects the wire medium supports two distinct P-polarized eigenwaves for a fixed direction of propagation [29,31]. In the above formulas, $k_t^2 = k_x^2 + k_y^2$. Thus, the electromagnetic field at any fixed cross section $z = z_0$, $0 < z_0 < L$ can be decomposed into a superposition of these eigenwaves. There are six waves in total as is seen from Eqs. (9) and (10): three waves propagating in the positive direction of the z axis and three waves propagating in the opposite direction.

Before going into the details of the Casimir energy calculation, we demonstrate that the "internal" reflection coefficient of the P-polarized eigenwaves (10) at an interface of the nanowire slab with air is indeed positive and approaches unity for one of these transverse magnetic (TM) waves when $k_t \gg |\omega/c|$. Although the scattering of waves by an interface formed by abruptly cutting the metallic wires has been considered before, to the best of our knowledge the case of internal reflection (i.e., when the incident wave propagates inside the nanowires) has not been yet studied analytically. Therefore, in the appendix we derive the complete reflection matrix [Eq. (A21)] for this case. For the purpose of illustration, here we select only the diagonal r^{p11} and r^{p22} components of this matrix. These components correspond to reflection of the two P-polarized eigenwaves into the same eigenwaves.

The dependence of these reflection coefficients on k_t is shown in Fig. 2. The plotted curves are for imaginary frequencies $\omega = i\xi$ that correspond to four values of the parameter $b\xi/c$ indicated in the figure caption. As one can see, the reflection coefficients of both modes are positive. When k_t increases, the reflection coefficient of the first P-polarized mode (the TM mode) decreases with k_t. Since this mode is cut off at low (real-valued) frequencies, its contribution to the Casimir force is irrelevant at distances larger than the period of the array [23]. On the other hand, the reflection coefficient of the second P-polarized mode (the quasi-TEM

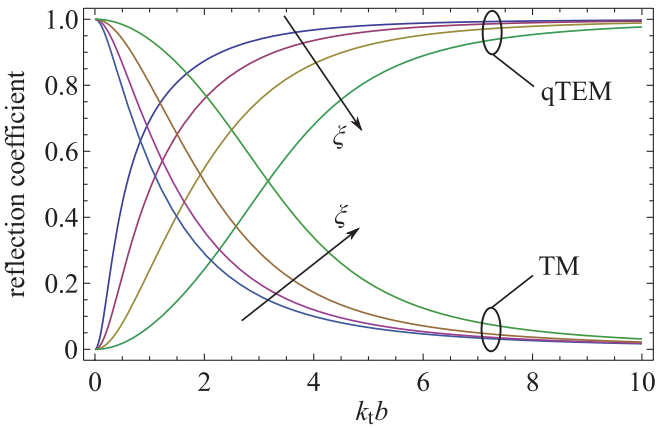

FIG. 2. (Color online) Reflection coefficients for the two P-polarized waves (indicated by TM and qTEM) incident on an interface of silver nanowires and air from within the nanowire slab as functions of the normalized transverse wave number. The plotted curves are for the imaginary frequencies $\omega = i\xi$, with the following values for the parameter $b\xi/c$: 0.25, 0.5, 1, and 2. The direction of increasing ξ is indicated by the arrows. In the calculations, $b = 200$ nm and $r_0 = 0.1b$.

mode, indicated as qTEM in the figure) increases with k_t and approaches unity when $k_t \gg \xi/c$. This is the mode that determines the intensity of the Casimir force when $a \gg b$. Thus, this example supports our initial idea that an interface of cut wires may effectively model a magnetic wall for the quasi-TEM waves, when $k_t \gg \xi/c$. It is important to mention that in the same manner as in an ideal magnetic wall, apart from small fluctuations in the vicinity of the wires, the tangential component of the magnetic field is near zero at the interface. Indeed, the magnetic field associated with a TEM mode is proportional to the current flowing in the wire, and since the currents vanish at the interface the magnetic field also does.

Next, we proceed with the calculation of the interaction energy (8). Let us represent the eigenwaves propagating in the positive z direction as E^+, and the waves propagating in the negative z direction as E^- (in the basis of the eigenwaves, $E^\pm$ are simply 3×1 column vectors with the complex amplitudes of the eigenwaves; see the appendix). Then, the amplitudes of the eigenwaves at two arbitrary cross sections $z = z_1$ and $z = z_2$, $0 < z_1 < z_2 < L$, are linked by the transfer matrix

$$\begin{pmatrix} E_1^+ \\ E_1^- \end{pmatrix} = \begin{pmatrix} \hat{\tau}_{++} & \hat{\tau}_{+-} \\ \hat{\tau}_{-+} & \hat{\tau}_{--} \end{pmatrix} \cdot \begin{pmatrix} E_2^+ \\ E_2^- \end{pmatrix}, \tag{11}$$

where the operators $\hat{\tau}_{\pm\pm}$ describe the interaction between the waves in the two regions.

It is obvious that the total transfer matrix for the structure shown in Fig. 1, written in terms of the wave amplitudes calculated at the planes $z_1 = 0^+$ and $z_2 = L^-$, is an ordered product of the transfer matrices of the layers and of the discontinuity planes:

$$\mathcal{T} = \mathcal{T}_A \cdot \mathcal{T}_{AB} \cdot \mathcal{T}_B \cdot \mathcal{T}_{BC} \cdot \mathcal{T}_C. \tag{12}$$

The matrices $\mathcal{T}_A$, $\mathcal{T}_B$, and $\mathcal{T}_C$ are diagonal and formed by the exponential propagators of the eigenwaves in each uniform region (the two regions of nanorods and the piston). The matrices $\mathcal{T}_{AB}$ and $\mathcal{T}_{BC}$ can be found from a complete set of the boundary conditions at an interface between two slabs of nanorods (one of them represents the piston). The details of this calculation are given in the appendix.

At the planes $z = 0$ and $z = L$, the waves are reflected so that we can write

$$E_1^+ = \hat{\rho}_1 E_1^-, \quad E_2^- = \hat{\rho}_2 E_2^+, \tag{13}$$

where $\hat{\rho}_{1,2}$ are the reflection operators defined at the planes where the nanorods are cut. These operators can be found from the known boundary conditions at the ends of the nanorods (see the appendix) [34,35]. Although in our structure $\hat{\rho}_1 = \hat{\rho}_2 = \hat{\rho}$, we want for the time being to keep (13) in a general form.

Using now Eq. (11) (with the global transfer matrix $\mathcal{T}$) and Eq. (13), it is possible to obtain after some manipulations a homogeneous system of the form $\hat{M} E_2^+ = 0$. This yields the characteristic equation of the normal modes of the whole structure:

$$\det\{\hat{\tau}_{++} + \hat{\tau}_{+-}\hat{\rho}_2 - \hat{\rho}_1\hat{\tau}_{-+} - \hat{\rho}_1\hat{\tau}_{--}\hat{\rho}_2\} = 0. \tag{14}$$

Using the fact that $\mathcal{T}_A$ and $\mathcal{T}_C$ are diagonal and have the form $\mathcal{T}_A = [\hat{\Lambda}_1^{-1}, 0; 0, \hat{\Lambda}_1]$, $\mathcal{T}_C = [\hat{\Lambda}_2^{-1}, 0; 0, \hat{\Lambda}_2]$ (in this notation, the semicolon separates the first and second rows of the operator matrices, and the comma separates different elements within the same row), and $\det\{\hat{\Lambda}_{1,2}\} \neq 0$ (see the appendix), the characteristic equation can be reformulated as

$$\tilde{D}(a,\omega,k_x,k_y) \equiv \det\{\hat{\tau}_{++}^{(0)} + \hat{\tau}_{+-}^{(0)}\hat{\mathcal{R}}_2 - \hat{\mathcal{R}}_1\hat{\tau}_{-+}^{(0)} - \hat{\mathcal{R}}_1\hat{\tau}_{--}^{(0)}\hat{\mathcal{R}}_2\} = 0, \tag{15}$$

where $\hat{\mathcal{R}}_1 = \hat{\Lambda}_1\hat{\rho}_1\hat{\Lambda}_1$, $\hat{\mathcal{R}}_2 = \hat{\Lambda}_2\hat{\rho}_2\hat{\Lambda}_2$, and $\mathcal{T}^{(0)} = \mathcal{T}_{AB} \cdot \mathcal{T}_B \cdot \mathcal{T}_{BC} = [\hat{\tau}_{++}^{(0)}, \hat{\tau}_{+-}^{(0)}; \hat{\tau}_{-+}^{(0)}, \hat{\tau}_{--}^{(0)}]$ is the transfer matrix of the piston. Physically, Eq. (15) corresponds to redefining the reference planes of the reflection operators, so that they include the effect of propagation in the layers of nanorods adjacent to the piston. Notice that as required the poles of $\tilde{D}$ are independent of a, because the only operators that depend on the position of the piston are $\mathcal{T}_A$ and $\mathcal{T}_C$, and these operators have no poles in ω.

However, the function $\tilde{D}(a,\omega,k_x,k_y)$ as defined by (15) does not satisfy the first two conditions listed after Eq. (8) and therefore cannot be used directly in the calculation of the Casimir interaction energy. Indeed, when $\xi \to \infty$, the first term in (15), $\hat{\tau}_{++}^{(0)}$, grows exponentially. In order to overcome this difficulty, we normalize the left-hand side of the characteristic equation as follows:

$$D(a,\omega,k_x,k_y) = \det\{\hat{\tau}_{++}^{(0)}\}^{-1}\tilde{D}(a,\omega,k_x,k_y). \tag{16}$$

It is important that the normalization factor in (16) *does not depend on the position of the piston* and thus may only result in a shift of the origin of the energy (8); that is, it results in a renormalization of the energy. In other words, the proper normalization must not introduce poles (or zeros) that depend on the variable parameter a in the function $D(a,\omega,k_x,k_y)$, as these points would modify the dependence of the integral (8) with respect to a. Moreover, it can be seen that when (16) is substituted into (8), the renormalized energy $\delta\mathcal{E}_c$ is such that $\delta\mathcal{E}_c \to 0$ when both $a \to \infty$ and $L - a \to \infty$; that is, this energy has simple physical meaning of an interaction energy.

In the next section, we consider the limiting case of an ideally conducting piston sliding in a wire medium background, for which the characteristic equation simplifies, and some further analytical development becomes possible.

IV. CASIMIR PRESSURE ON A PERFECTLY CONDUCTING PISTON IN A WIRE MEDIUM BACKGROUND

A PEC piston can be modeled as a sheet of dielectric with $\varepsilon_h(i\xi) \to \infty$. It can be directly verified that the elements of the piston transfer matrix behave in this limit as $\hat{\tau}_{++}^{(0)} \sim \hat{\tau}_\infty$, $\hat{\tau}_{+-}^{(0)} \sim \hat{\tau}_\infty$, $\hat{\tau}_{-+}^{(0)} \sim -\hat{\tau}_\infty$, and $\hat{\tau}_{--}^{(0)} \sim -\hat{\tau}_\infty$, where $\hat{\tau}_\infty$ is the limiting form of all these operators. This form, in general, is such that $\det\{\hat{\tau}_\infty\} \to \infty$, when $\varepsilon_h(i\xi) \to \infty$. Thus, the characteristic Eq. (15) factorizes in this limit as

$$\det\{(\hat{1} + \hat{\mathcal{R}}_1)\hat{\tau}_\infty(\hat{1} + \hat{\mathcal{R}}_2)\} = 0, \tag{17}$$

and the function $D(a,\omega,k_x,k_y)$ reads, according to (16), as

$$D(a,\omega,k_x,k_y) = \det\{\hat{1} + \hat{\mathcal{R}}_1\}\det\{\hat{1} + \hat{\mathcal{R}}_2\} = \det\left\{\hat{1} + \hat{\rho}\,\hat{\Lambda}_1^2\right\}\det\left\{\hat{1} + \hat{\rho}\,\hat{\Lambda}_1^2\right\}, \quad (18)$$

where the last equality is obtained using the definitions of $\hat{\mathcal{R}}_{1,2}$ and the fact that $\det\{\hat{1} + \hat{\Lambda}_{1,2}\hat{\rho}_{1,2}\hat{\Lambda}_{1,2}\} = \det\{\hat{\Lambda}_{1,2}^{-1} + \hat{\rho}_{1,2}\hat{\Lambda}_{1,2}\}\det\{\Lambda_{1,2}\} = \det\{\hat{1} + \hat{\rho}_{1,2}\hat{\Lambda}_{1,2}^2\}$.

Such factorization has a simple physical meaning: the two regions $z < a$ and $z > a + h$ are electromagnetically screened one from another by a PEC piston and therefore behave independently. In such a case, the characteristic equation of the whole system must be a product of the two independent equations for the two separate regions. Hence, the Casimir energy of the whole system given by (8) is just a sum of the energies of the two regions.

Taking into account that $\hat{\Lambda}_1 = e^{-a\hat{\gamma}_z}$ and $\hat{\Lambda}_2 = e^{-(L-a-h)\hat{\gamma}_z}$, where $\hat{\gamma}_z = -i\hat{k}_z$ is the complex propagation factor operator (see the appendix), we can write for a PEC piston

$$D(a,\omega,k_x,k_y) = \det\{\hat{1} + \hat{\rho}\,e^{-2a\hat{\gamma}_z}\}\det\{\hat{1} + \hat{\rho}\,e^{-2(L-a-h)\hat{\gamma}_z}\}. \quad (19)$$

Therefore, the interaction part of the zero-point energy in this structure reads

$$\delta\mathcal{E}_c(a) = \mathcal{E}(a) + \mathcal{E}(L-a-h), \quad \text{where}$$
$$\mathcal{E}(z) = \frac{\hbar}{2\pi^3}\int_0^{\pi/b}\int_0^{\pi/b}\int_0^{\infty}\log\det\{\hat{1} + \hat{\rho}\,e^{-2z\hat{\gamma}_z}\}\,d\xi\,dk_x\,dk_y. \quad (20)$$

When $L \to \infty$, $\mathcal{E}(L-a-h) \to 0$ and $\delta\mathcal{E}_c(a) \to \mathcal{E}(a)$. At imaginary frequencies $\omega = i\xi$ the operators that occur in (20) are represented by real-valued matrices. Clearly, if the eigenvalues of the operator $\hat{\rho}\,e^{-2z\hat{\gamma}_z}$ are all real and non-negative, then the interaction energy is also non-negative: $\mathcal{E}(z) \geqslant 0$. At very small separations $z \to 0$, this operator reduces to the reflection operator $\hat{\rho}$. As shown in the appendix, the eigenvalues of $\hat{\rho}$ can be calculated in a closed analytical form, and they are, indeed, all real and non-negative when $\varepsilon_h(i\xi) \geqslant 1$ (because in the present paper ε_h is defined with respect to the vacuum permittivity ε_0 this condition is always observed due to Kramers-Kronig's formulas).

Moreover, in the important case in which $\varepsilon_h = 1$ and z increases, the eigenvalues of the operator $\hat{\rho}e^{-2z\hat{\gamma}}$ change with z but remain real and non-negative, as proven in the appendix. Given that from physical reasons the interaction energy in our structure must decrease in absolute value with the increase of z (here we consider the function $\mathcal{E}(z)$ as defined by (20), i.e., the Casimir energy with respect to a single interface), the sign of $\mathcal{E}(z)$ determines the sign of the Casimir force acting on the piston. Hence, the positive $\mathcal{E}(z)$ corresponds to repulsion in this case. Thus, even when $\varepsilon_h = 1$ (host medium is air), the piston slides on the nanorods as if it were repelled by an ideal PMC wall.

The Casimir pressure on the piston can be calculated by differentiating (20) with respect to the position of the piston $z = a$: $F_c(a) = -d\,\delta\mathcal{E}_c(a)/da$. Under this definition, the positive direction for the force coincides with the direction of the z axis. In the case of the PEC piston, the differentiation can be done in a closed form using Jacobi's formula $d(\det\hat{A}) = \mathrm{tr}\{\hat{A}^{-1}d\hat{A}\}\det\{\hat{A}\}$:

$$F_c(a) = F(a) - F(L-a-h), \quad \text{where}$$
$$F(z) = \frac{\hbar}{\pi^3}\int_0^{\pi/b}\int_0^{\pi/b}\int_0^{\infty} \times \mathrm{tr}\{(\hat{1} + \hat{\rho}e^{-2z\hat{\gamma}_z})^{-1}\hat{\rho}e^{-2z\hat{\gamma}_z}\hat{\gamma}_z\}d\xi\,dk_x\,dk_y, \quad (21)$$

where $\mathrm{tr}\{\ldots\}$ denotes the trace of an operator. When $L \to \infty$, $F_c(a) \to F(a)$, because $F(L-a-h) \to 0$ in this limit. A negative $F(z)$ means that the piston attracts to the nearby ends of the nanorods, while a positive $F(z)$ corresponds to a repulsive force that pushes the piston toward the geometrical center of the structure.

In the numerical examples given in the next section, we calculate the Casimir energy and the force acting on different pistons in silver and PEC nanorods.

V. NUMERICAL EXAMPLES AND DISCUSSION

In the first numerical example, we calculate the Casimir interaction energy for several types of conducting pistons embedded in silver (Ag) or PEC nanorods, by direct numerical integration of (8) [we use (20) for the PEC pistons]. We do this for the following values of the geometrical parameters (Fig. 1): separation of the nanorods $b = 200$ nm, radius of the nanorods $r_0 = 0.1b$, length of the nanorods $L = 20\,b$, and piston thickness $h = b$. Although this is not crucial in the calculations, the host material is assumed to be vacuum or air: $\varepsilon_h = 1$ (to model this situation in practice, the ends of the nanorods may be mechanically attached to thin sheets of low permittivity dielectrics; the effect of such sheets on the Casimir energy is negligible at distances larger than the thickness of the sheets; we give more detail on this later in the text). We consider pistons made of tungsten (W), copper (Cu), and PEC. The response of metals at imaginary frequencies is calculated from the respective Drude models [36] (which may not be rigorously valid at low temperatures; however, as argued in [37], they still yield physically sound results up to moderate separations); that is, the dispersion and loss of real metals is taken into account. It is worth noting that when $\varepsilon_h = 1$ the quantum fluctuations of the electromagnetic field associated with S-polarized normal modes do not contribute to the Casimir force acting on the piston in the limit of vanishingly thin wires. Thus, the dominant contribution to the Casimir force is due to the oscillators associated with the P-polarized normal modes for which the interfaces $z = 0$ and $z = L$ effectively behave as PMC walls.

The results of the calculations are represented in Fig. 3. As can be seen, the interaction energy is strictly positive in all the scenarios considered here. When the distance to the closest air interface increases, the energy decreases and has a minimum at $a/b = (L-h)/(2b) = 9.5$, that is, when the piston is exactly at the center of the nanowire structure. Hence, the quantum fluctuations of the electromagnetic field in all the cases represented in Fig. 3 (excluding the curve with label "Diel," which is discussed ahead) result in repulsive forces that push the piston toward the geometrical center of the

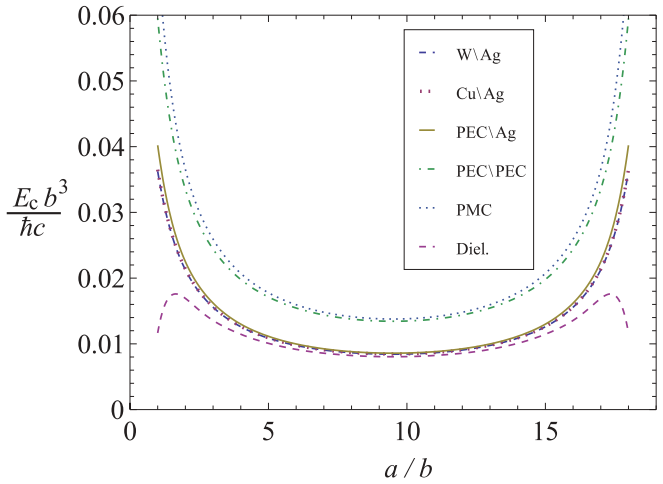

FIG. 3. (Color online) The normalized Casimir interaction energy in the system shown in Fig. 1 as a function of the relative separation a/b. The following combinations are considered: W\Ag, tungsten piston sliding on silver nanorods; Cu\Ag, copper piston sliding on silver nanorods; PEC\Ag, PEC piston sliding on silver nanorods; PEC\PEC, PEC piston sliding on PEC nanorods; and PMC, PEC piston sliding on PEC nanorods with ideal PMC walls at $z = 0$ and $z = L$. The bottom curve marked as "Diel." is explained in the main text. The values of the parameters are $b = 200$ nm, $r_0 = 0.1\,b$, $L = 20\,b$, and $h = b$ (see Fig. 1).

structure. This middle point is the point of a stable equilibrium with respect to the piston movements along the z axis. It is worth noting that there is no contradiction between our theory and the recent findings by Rahi *et al.* [38] that forbid stable arrangements of interacting metal-dielectric bodies in a vacuum. In our case, a stable equilibrium exists because we limit the relative movement of the bodies (precisely, we fix the nanorods, and the piston is able to slide *only along* them but not in directions in the xoy plane). On the other hand, the theory of Rahi *et al.* only applies to the case of unconstrained displacements. A simple electrostatic analog of our system is shown in the lower panel of Fig. 1.

Another argument in support of our result is that, from a macroscopic point of view, the piston in our system is moving not in vacuum but effectively in a cavity filled with a medium characterized by the dyadic permittivity (7). It is known that for dielectric bodies moving in cavities filled with dielectric fluids, stable arrangements are possible [13,14].

In order to estimate how well the interface of cut nanorods models the PMC condition, we have calculated the interaction energy of a PEC piston sliding in PEC nanorods terminated with ideal PMC walls (the upper curve in Fig. 3 marked as "PMC"). This calculation is done based on the expression for the TEM contribution to the Casimir force (1). As can be seen, the energy in a structure with freestanding cut nanorods (the curve marked as "PEC\PEC") is practically the same as for an idealized PMC-terminated structure. Thus, an interface with abruptly cut nanorods mimics a PMC wall with high accuracy.

As can be seen from Fig. 3, the dispersion in both the piston and the nanowires made of real metals reduces the interaction energy. However, the most significant reduction happens due to the dispersion of the thin nanowires. When the nanowire radius becomes comparable to the plasma skin depth $\delta_p \sim c/\omega_p$ (ω_p is the plasma frequency of the metal), the high-frequency normal oscillations of a nanowire crystal contribute less to the electromagnetic part of the zero-point energy, because the total zero-point energy has a component associated with the kinetic energy of moving electrons. At small and medium separations, this effect is dominant and is responsible for a significant decrease in the value of the interaction energy in our structure when the PEC nanowires are replaced by silver nanowires.

It is worth noting here that at large separations the Casimir energy is mostly determined by the response at low frequencies $\xi \lesssim c/a$ and thus, at large separations that we do not consider in this paper, by imaginary frequencies such that $\xi \lesssim c/a \lesssim \Gamma$, where Γ is the collision frequency of metal from which the nanorods are made. At this point, it is of critical importance to know accurately the limiting value of Γ at zero temperature. In fact, up to the present day there is a lingering controversy in the literature on the type of dispersion models for real metals that should be used in Casimir force calculations at low temperatures [37,39–42]. However, the results of this paper are not affected by this controversy because we deal with ultralong-range forces emerging from the (quasi)-TEM modes. Indeed, the origin of the controversy is in different reflectivities of the plates predicted by the Drude model and the lossless plasma model for the TE modes in the limit of zero frequency. In our system, the effect of the TE modes is negligible (they do not interact with the thin nanowires and are not reflected at the nanowire-air interface). On the other hand, the reflectivity of the TEM modes is the same for both models [23]: $\rho = (1 - \sqrt{\varepsilon_r(i\xi)})/(1 + \sqrt{\varepsilon_r(i\xi)}) \to -1$, when $\varepsilon_r(i\xi) \to \infty$.

It is also seen from Fig. 3 that the conductivity of the piston has a much smaller influence on the value of the Casimir energy than the conductivity of the nanorods. In fact, the curves for tungsten and copper pistons practically coincide, despite a significant difference in the plasma frequency of these metals, and are very close to the curve for the PEC piston. This agrees perfectly with the estimations done in our previous work [23], where it was found that at separations on the order of microns the plates made of real metals behave closely to PEC when Casimir forces in nanowires are considered.

Next, we calculate the Casimir force per unit area (the pressure) acting on either a metallic or a PEC piston sliding in the same structure as before. The force is calculated by differentiating the interaction energy with respect to the separation a [for the PEC pistons, the pressure is calculated from (21)]. The results of these calculations are depicted in Fig. 4.

As can be seen, the force acting on the piston is positive at $a < (L - h)/2$ and negative at $a > (L - h)/2$; that is, it is always directed toward the equilibrium point at the geometrical center of the structure. Away from the equilibrium point, the force is repulsive and behaves as $1/d^2$, where d is the distance to the neighboring ends of the nanorods: $d = a$, when $a \ll L - a - h$, and $d = L - a - h$, when $L - a - h \ll a$ (see the inset of Fig. 4, which demonstrates that the force decays by a factor of about $\sim 0.05/0.002 = 25$ when the distance is varied by a factor of 5). This further supports the statement that the forces considered in this paper are of the same nature

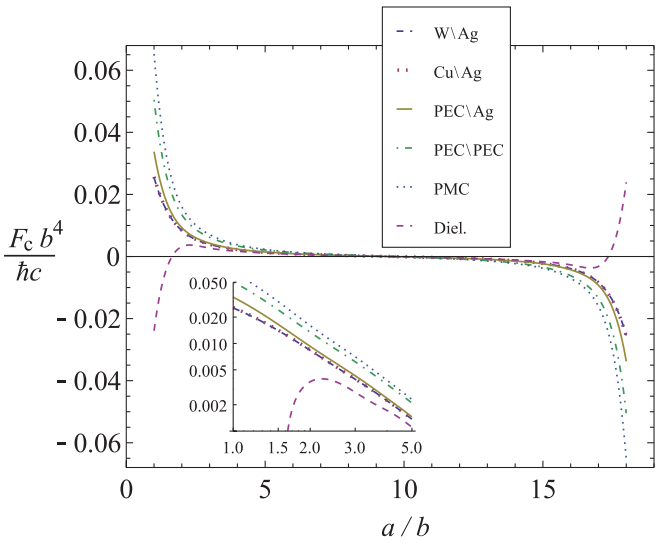

FIG. 4. (Color online) The normalized Casimir pressure on metallic and PEC pistons in the structure shown in Fig. 1 as a function of the relative separation a/b. The sign of the pressure is with respect to the z axis. The inset shows the same pressure in logarithmic scale, for the range of separations $1 \leqslant a/b \leqslant 5$, which confirms the characteristic $1/a^2$ decay of the force. The plot legend is the same as in Fig. 3.

as the ultralong-range Casimir-Lifshitz forces that we have investigated in Ref. [23].

The finite conductivity of real metals affects the Casimir pressure on the piston in the same manner as it affects the Casimir energy. One can see that the reduction in the value of the force is mainly due to the dispersion in thin nanorods, while at small separations the effect of the finite conductivity of the piston is also noticeable, which is in perfect agreement with our previous findings on attractive Casimir forces acting on metallic plates in silver nanorods [23].

In Sec. IV, our theoretical calculations assumed an infinitesimal gap between the nanorods and the piston body, but in a realistic structure this gap is necessarily finite. This will result in a lower value of the Casimir pressure on the piston when compared to the ideal case. This decrease, however, is not dramatic, as is seen from the following calculation. To account for the gaps, one may consider the jump in the characteristic impedance that is seen by a TEM wave propagating along a nanorod and entering a gap. The characteristic impedance of a single unit cell of a nanowire crystal is $Z_0 = \sqrt{L_0/C_0} = (\eta_0/2\pi)\log[b^2/4r_0(b-r_0)]$ (see [31]), while the characteristic impedance of a nanowire entering into a round hole in the piston may be estimated with the well-known formula for a coaxial cable: $Z_h = (\eta_0/2\pi)\log(r_h/r_0)$, where $r_h > r_0$ is the hole radius (the nanowires and the piston are assumed highly conducting), and $\eta_0 = \sqrt{\mu_0/\varepsilon_0}$. Thus, the ratio of the two impedances that determines the magnitude of the reflection coefficient of the TEM waves at the piston is $Z_h/Z_0 = \log(r_h/r_0)/\log[b^2/4r_0(b-r_0)]$. For the case of a rather large 50% gap ($r_h = 1.5r_0$), we obtain $Z_h/Z_0 \approx 0.17$, which corresponds to the reflection coefficient $\rho = (Z_h/Z_0 - 1)/(Z_h/Z_0 + 1) \approx -0.7$, that is, only about 30% lower in absolute value than in the ideal case with no gap. As the Casimir pressure is roughly proportional to this reflection coefficient [Eq. (1)], one may expect a similar reduction in its value.

It is interesting to compare the absolute value of the repulsive Casimir force with other forces that may act on the piston in a realistic structure. For example, it is instructive to compare the Casimir force with the gravitational force acting on the piston in a configuration in which the nanowires are vertically aligned. The gravitational force per unit area of the piston in this configuration is $F_G = g\rho_{mat}h$, where $g \approx 9.8$ m s^{-2} is the acceleration of free fall, ρ_{mat} is the mass density of the piston, and h is the piston thickness. For the parameters used in Figs. 3 and 4, assuming the piston made of tungsten ($\rho_{mat} \approx 19.25 \times 10^3$ kg m^{-3}), one finds $F_G \approx 3.8 \times 10^{-2}$ N m^{-2}, which in the dimensionless units of Fig. 4 is $F_G b^4/(\hbar c) \approx 1.9 \times 10^{-3}$. From the inset plot of Fig. 4, we realize that the repulsive Casimir force in our configuration is strong enough to lift the piston to about one micrometer above the tips of the nanorods!

In a structure with horizontally oriented nanorods, there may be some elastic deformation due to the weight of the piston. The maximal deformation of a single nanorod (assuming that the piston is in the middle of the structure) can be estimated [43] as $\delta_{max} = PL^3/(48EI)$, where P is the piston weight per a single nanorod, $P = g\rho_{mat}hb^2$, L is the length of the nanorods (the nanorods are assumed to be simply supported at both ends), E is the effective Young modulus of nanorod's material, and $I = \pi r_0^4/4$ is the moment of inertia of a rod with a circular cross section. For silver nanorods with radius on the order of tens of nanometers, the bulk value of Young's constant for silver [44] may be used: $E = 83 \times 10^9$ N m^{-2}, from which we obtain $\delta_{max} \approx 0.19$ pm for the structure with a tungsten piston. Such a small deformation may be safely neglected.

Other forces that are of importance in a real structure are the stiction forces at the nanoholes of the perforated piston. To allow for a movement, the nanoholes must have larger radii than the nanorods. Still, a nonideally aligned nanorod may touch the walls of the associated nanohole at some points. An estimation of the contact area at these points is difficult since there are virtually no experiments on stiction of metallic nanorods in nanoholes in metallic bodies. For instance, strong enough adhesion may result in a deformation of the nanorod so that the contact area is larger than it would be for a nondeformed nanorod. Therefore, instead of obtaining the contact area in a particular contact scenario, we estimate the maximum allowable total contact area by equating the Casimir force per nanorod to the stiction force acting on the same nanorod.

This is done as follows. First, using Eq. (1), we may express the ratio of the Casimir force to the stiction force per a single nanorod as $|F_{TEM}/F_{st}| = \pi\hbar c/(48a^2\sigma_{sh}A_c)$, where σ_{sh} is the average sheer stress at the points of contact and A_c is the total contact area. From here, $A_c = \pi\hbar c/(48a^2\sigma_{sh}|F_{TEM}/F_{st}|)$. The sheer stress due to adhesion can be estimated very roughly from the data of Refs. [45–47] as being of order of $\sigma_{sh} \approx 10^6$ N m^{-2}. Demanding that $|F_{TEM}/F_{st}| \gtrsim 2$ and $a \approx 0.5$ μm, we obtain for the contact area $A_c \lesssim 4 \times 10^{-3}$ nm^2, which is, for all practical reasons, prohibitively small if each nanorod is allowed to adhere to the piston body. However, if only a fraction of the nanorods is in an adhesive contact with the

piston (i.e., their respective holes are made tighter than of the most of others; these nanorods may serve as mechanical support for the rest of the structure), then the Casimir force may outweigh the stiction forces. For example, if there is a single adherent nanorod per 50×50 array of other nanorods, then the contact area of this nanorod may be of order of 10^{-17} m^2, which corresponds to a square area of about 3×3 nm^2. Nevertheless, the above estimations show that adhesion of the nanorods to the piston body must be avoided as much as possible.

It should be also noted that in the presence of the gaps there exists a Casimir attraction between the nanorods and the walls of the piston nanoholes. These attractive forces act radially and compensate each other when the nanorods are ideally centered within their nanoholes. A realistic fabrication process, however, will result in nanorods slightly shifted from their symmetric positions. Thus, in each unit cell there will appear a radial Casimir force that will try to displace the nanorod even further away from the hole center.

It is possible to estimate the width of the gap at which the radial Casimir forces may be compensated by the elasticity of the nanorods. Within the proximity-force approximation, the radial Casimir force between two eccentric highly conducting cylinders is, in our notations, $F_{\mathrm{PFA}} = h\delta(\pi^3\hbar c/60r_0^4)/[(r_{\mathrm{h}}/r_0) - 1]^5$ (Ref. [48]), where δ is the offset of a nanorod from its symmetric position. Equating this to the elastic force $F_{\mathrm{e}} = 12\pi r_0^4 E\delta/L^3$ (this case is analogous to the deformation due to the gravitational force that we considered above), we find that the two forces are equal if $[(r_{\mathrm{h}}/r_0) - 1]^5 = \pi^2\hbar c L^3 h/(12 \times 60 r_0^8 E)$. Substituting the parameters of our structure into this formula, we find $r_{\mathrm{h}}/r_0 \approx 2.2$, which corresponds to a rather large gap. To achieve a stable configuration with a 50% gap, the nanorod radius must be increased at least up to $r_0 \approx 35$ nm.

Finally, to estimate the influence of supporting dielectric layers, we have calculated the Casimir energy and the pressure for the structure shown in Fig. 1, assuming that the ends of silver nanorods are attached to silica ($\varepsilon_{\mathrm{h}} \approx 2.08$) layers of thickness $d = 0.5b = 100$ nm (in our model the nanowires are prolonged into the silica slabs). The piston is modeled as an ideal PEC material. The calculated results are represented in Figs. 3 and 4 by the curves marked as "Diel." As could be expected, at small separations the piston is attracted to the silica layers. Notice that in this configuration the *S*-polarized waves play a role in the sign of the Casimir force because they are reflected by the silica layers: They promote the attraction of the piston and the silica layers. However, at separations significantly larger than d, the piston is pushed toward the geometrical center of the structure, as in the cases without the layers. Indeed, the contribution of the *S*-polarized waves to the Casimir force is short range, unlike the contribution of the *P*-polarized waves [23].

VI. CONCLUSIONS

In this work, we have studied the Casimir force acting on a piston sliding in a background formed by a uniaxial arrangement of cut metallic nanorods. It was shown that in such an environment it is possible to mimic the behavior of a PMC wall simply by cutting the wires at a desired plane. Hence, it is expected that a metal-dielectric body placed inside the structure will be repelled away from the interfaces with air (i.e., the effective "PMC walls"), even if the nanowires stand in a vacuum. For simplicity, the analysis of this work was restricted to either semitransparent or PEC pistons. Consistent with our intuition, it was found that such pistons are pushed toward the geometrical center of the structure, which is shown to be a point of a stable equilibrium. Our results do not contradict to the recent theorem by Rahi *et al.* [38] that establishes that there is no stable equilibrium in an arrangement of metal-dielectric bodies interacting in a vacuum. Unlike the situation considered by Rahi *et al.*, in our system the relative movement of bodies is limited: We assume that the movement of the piston is constrained to the direction parallel to the nanowires.

The nature of the repulsive force exerted on the metallic piston studied in this paper is the same as that of the ultralong-range forces that we have considered in our recent work [23]. Thus, the force between planar slabs embedded in a wire medium background varies with the distance, a, as $1/a^2$, as compared to $1/a^4$ in similar structures in a vacuum. Finally, we note that the described effect of repulsion with respect to the interface of cut nanowires could also be interpreted (from a microscopic, rather than from an effective medium perspective) as an effect of attraction of the piston by the nanowires.

APPENDIX

On the basis of *S*- and *P*-polarized eigenwaves, the forward- and backward-propagating wave amplitudes $E^{\pm}$ at an arbitrary cross section of the structure can be written as $E^{\pm} = E^{\mathrm{s}\pm} + \eta_0 H^{\mathrm{p}\pm}$, where the column vectors

$$E^{\mathrm{s}\pm} = (A^{\mathrm{s}\pm},0,0)^{\mathrm{T}}, \quad \eta_0 H^{\mathrm{p}\pm} = (0, A^{\mathrm{p1}\pm}, A^{\mathrm{p2}\pm})^{\mathrm{T}} \tag{A1}$$

store the complex amplitudes of the electric field of the *S*-polarized wave and the magnetic field (multiplied by $\eta_0 = \sqrt{\mu_0/\varepsilon_0}$) of the *P*-polarized waves, respectively (it is convenient to use the magnetic field for the *P*-polarized waves because its tangential component does not vary with the angle of incidence). The matrices $\mathcal{T}_A$, $\mathcal{T}_B$, and $\mathcal{T}_C$ are thus simple diagonal block matrices in this basis:

$$\mathcal{T}_{A,B,C} = \begin{pmatrix} e^{-ih_{A,B,C}\hat{k}_z} & 0 \\ 0 & e^{+ih_{A,B,C}\hat{k}_z} \end{pmatrix}, \tag{A2}$$

where $h_{A,B,C}$ is the geometrical thickness of the corresponding layer and $\hat{k}_z$ is a 3×3 diagonal matrix that holds the propagation factors $k_z^{\mathrm{s,p1,p2}}$, $\mathrm{Im}(k_z^{\mathrm{s,p1,p2}}) \geqslant 0$, of the three positively propagating eigenwaves of a layer: one for the *S*-polarized wave and two for the *P*-polarized waves, as is given by (9) and (10).

It is also clear that the operators $\hat{\tau}_{\pm\pm}$ of the total transfer matrix (12) must have the following matrix representation when expressed on the basis of *S*- and *P*-polarized

eigenwaves:

$$\hat{\tau}_{\pm\pm} = \begin{pmatrix} t^{\mathrm{s}}_{\pm\pm} & 0 & 0 \\ 0 & t^{\mathrm{p11}}_{\pm\pm} & t^{\mathrm{p12}}_{\pm\pm} \\ 0 & t^{\mathrm{p21}}_{\pm\pm} & t^{\mathrm{p22}}_{\pm\pm} \end{pmatrix}. \tag{A3}$$

This form implies that the *S*- and *P*-polarized waves do not interact in the structure that we consider.

The components of the matrices $\mathcal{T}_{AB}$ and $\mathcal{T}_{BC}$ have the same form (A3) and can be found from the boundary conditions at an interface between two layers of nanorods with different permittivities of the host material. As follows from our recent work [49], due to the effects of spatial dispersion in the nanowire material, the complete set of boundary conditions at such an interface includes a pair of additional boundary conditions that are written in terms of the averaged current density in the nanorods:

$$\hat{\mathbf{z}} \cdot (\mathbf{J}_1 - \mathbf{J}_2) = \mathbf{0}, \quad \hat{\mathbf{z}} \cdot \left[\frac{1}{\varepsilon_{\mathrm{h1}}} \frac{\partial \mathbf{J}_1}{\partial z} - \frac{1}{\varepsilon_{\mathrm{h2}}} \frac{\partial \mathbf{J}_2}{\partial z} \right] = 0. \tag{A4}$$

The first condition in this pair is simply the continuity of the z component of the current across the interface, while the second one is related with the continuity of the effective potential of a nanorod. As usual, one should also impose the continuity of the tangential components of the electric and magnetic fields at an interface:

$$\hat{\mathbf{z}} \times (\mathbf{E}_1 - \mathbf{E}_2) = \mathbf{0}, \quad \hat{\mathbf{z}} \times (\mathbf{H}_1 - \mathbf{H}_2) = \mathbf{0}. \tag{A5}$$

It can be proven that for plane waves with fixed $\mathbf{k}_{\mathrm{t}}$, the z component of the current density can be expressed as

$$J_z = \frac{i\mathbf{k}_{\mathrm{t}}}{k_{\mathrm{t}}^2} \cdot \left[\frac{\partial^2 \mathbf{H}_{\mathrm{t}}}{\partial z^2} + (\beta^2 - k_{\mathrm{t}}^2)\mathbf{H}_{\mathrm{t}} \right]. \tag{A6}$$

Thus, taking into account (A5) and (A6), the additional boundary conditions (A4) can be rewritten in terms of the tangential field components:

$$\hat{\mathbf{v}} \cdot \left[\frac{\partial^2 \mathbf{H}_{\mathrm{t1}}}{\partial z^2} + \beta_1^2 \mathbf{H}_{\mathrm{t1}} \right] = \hat{\mathbf{v}} \cdot \left[\frac{\partial^2 \mathbf{H}_{\mathrm{t2}}}{\partial z^2} + \beta_2^2 \mathbf{H}_{\mathrm{t2}} \right], \tag{A7}$$

$$\hat{\mathbf{u}} \cdot \left[\frac{\partial^2 \mathbf{E}_{\mathrm{t1}}}{\partial z^2} + \beta_1^2 \mathbf{E}_{\mathrm{t1}} \right] = \hat{\mathbf{u}} \cdot \left[\frac{\partial^2 \mathbf{E}_{\mathrm{t2}}}{\partial z^2} + \beta_2^2 \mathbf{E}_{\mathrm{t2}} \right]. \tag{A8}$$

where $\hat{\mathbf{u}} = \mathbf{k}_{\mathrm{t}}/|\mathbf{k}_{\mathrm{t}}|$ and $\hat{\mathbf{v}} = \hat{\mathbf{z}} \times \hat{\mathbf{u}}$. As is seen, the additional boundary conditions are only relevant for the *P*-polarized waves.

With the notations introduced above, the tangential vector fields at the two sides of an interface (marked with an index $m = 1,2$; without any loss of generality, here we let the interface be at $z = 0$) satisfy

$$\mathbf{E}_{tm} = \left(\hat{\mathbf{v}}, \kappa^{\mathrm{p1}}_{z,m} \varepsilon^{-1}_{\mathrm{h}m} \hat{\mathbf{u}}, \kappa^{\mathrm{p2}}_{z,m} \varepsilon^{-1}_{\mathrm{h}m} \hat{\mathbf{u}}\right) \cdot (e^{iz\hat{k}_{z,m}} E^+_m + e^{-iz\hat{k}_{z,m}} E^-_m), \tag{A9}$$

$$\eta_0 \mathbf{H}_{tm} = \left(-\kappa^{\mathrm{s}}_{z,m} \varepsilon^{-1}_{\mathrm{h}m} \hat{\mathbf{u}}, \hat{\mathbf{v}}, \hat{\mathbf{v}}\right) \cdot (e^{iz\hat{k}_{z,m}} E^+_m - e^{-iz\hat{k}_{z,m}} E^-_m), \tag{A10}$$

where $\kappa^{\mathrm{s,p1,p2}}_{z,m} = k^{\mathrm{s,p1,p2}}_{z,m}/(\omega\sqrt{\varepsilon_0\mu_0})$, and the dot product is understood as $(\mathbf{a},\mathbf{b},\mathbf{c}) \cdot (A^{\mathrm{s}\pm}, A^{\mathrm{p1}\pm}, A^{\mathrm{p2}\pm})^{\mathrm{T}} = \mathbf{a}A^{\mathrm{s}\pm} + \mathbf{b}A^{\mathrm{p1}\pm} + \mathbf{c}A^{\mathrm{p2}\pm}$. Substituting the expressions (A9) and (A10) into the boundary conditions (A5)–(A8), we obtain a system of six linear equations for the twelve complex amplitudes $A^{\mathrm{s,p1,p2}\pm}_{1,2}$. The transfer matrix in question is then found by solving for six unknown amplitudes $A^{\mathrm{s,p1,p2}\pm}_1$ in terms of the other six given amplitudes $A^{\mathrm{s,p1,p2}\pm}_2$. Below we give the result for the components of $\mathcal{T}_{AB} = [\hat{\tau}_{++}, \hat{\tau}_{+-}; \hat{\tau}_{-+}, \hat{\tau}_{--}]$, which are all of the form (A3) ($m = 1$ for layer A and $m = 2$ for layer B):

$$t^{\mathrm{s}}_{++} = t^{\mathrm{s}}_{--} = \frac{\kappa^{\mathrm{s}}_{z,1} + \kappa^{\mathrm{s}}_{z,2}}{2\kappa^{\mathrm{s}}_{z,1}}, \tag{A11}$$

$$t^{\mathrm{s}}_{+-} = t^{\mathrm{s}}_{-+} = \frac{\kappa^{\mathrm{s}}_{z,1} - \kappa^{\mathrm{s}}_{z,2}}{2\kappa^{\mathrm{s}}_{z,1}}, \tag{A12}$$

$$t^{\mathrm{p11}}_{++} = t^{\mathrm{p11}}_{--} = \frac{\left(\varepsilon_{\mathrm{h2}}\kappa^{\mathrm{p1}}_{z,1} + \varepsilon_{\mathrm{h1}}\kappa^{\mathrm{p1}}_{z,2}\right)\left[(\varepsilon_{\mathrm{h1}} - \varepsilon_{\mathrm{h2}}) + \left(\kappa^{\mathrm{p1}}_{z,2} - \kappa^{\mathrm{p2}}_{z,1}\right)\left(\kappa^{\mathrm{p1}}_{z,2} + \kappa^{\mathrm{p2}}_{z,1}\right)\right]}{2\varepsilon_{\mathrm{h2}}\kappa^{\mathrm{p1}}_{z,1}\left(\kappa^{\mathrm{p1}}_{z,1} - \kappa^{\mathrm{p2}}_{z,1}\right)\left(\kappa^{\mathrm{p1}}_{z,1} + \kappa^{\mathrm{p2}}_{z,1}\right)}, \tag{A13}$$

$$t^{\mathrm{p12}}_{++} = t^{\mathrm{p12}}_{--} = \frac{\left(\varepsilon_{\mathrm{h2}}\kappa^{\mathrm{p1}}_{z,1} + \varepsilon_{\mathrm{h1}}\kappa^{\mathrm{p2}}_{z,2}\right)\left[(\varepsilon_{\mathrm{h1}} - \varepsilon_{\mathrm{h2}}) + \left(\kappa^{\mathrm{p2}}_{z,2} - \kappa^{\mathrm{p2}}_{z,1}\right)\left(\kappa^{\mathrm{p2}}_{z,2} + \kappa^{\mathrm{p2}}_{z,1}\right)\right]}{2\varepsilon_{\mathrm{h2}}\kappa^{\mathrm{p1}}_{z,1}\left(\kappa^{\mathrm{p1}}_{z,1} - \kappa^{\mathrm{p2}}_{z,1}\right)\left(\kappa^{\mathrm{p1}}_{z,1} + \kappa^{\mathrm{p2}}_{z,1}\right)}, \tag{A14}$$

$$t^{\mathrm{p21}}_{++} = t^{\mathrm{p21}}_{--} = \frac{\left(\varepsilon_{\mathrm{h2}}\kappa^{\mathrm{p2}}_{z,1} + \varepsilon_{\mathrm{h1}}\kappa^{\mathrm{p1}}_{z,2}\right)\left[(\varepsilon_{\mathrm{h2}} - \varepsilon_{\mathrm{h1}}) + \left(\kappa^{\mathrm{p1}}_{z,1} - \kappa^{\mathrm{p1}}_{z,2}\right)\left(\kappa^{\mathrm{p1}}_{z,1} + \kappa^{\mathrm{p1}}_{z,2}\right)\right]}{2\varepsilon_{\mathrm{h2}}\kappa^{\mathrm{p2}}_{z,1}\left(\kappa^{\mathrm{p1}}_{z,1} - \kappa^{\mathrm{p2}}_{z,1}\right)\left(\kappa^{\mathrm{p1}}_{z,1} + \kappa^{\mathrm{p2}}_{z,1}\right)}, \tag{A15}$$

$$t^{\mathrm{p22}}_{++} = t^{\mathrm{p22}}_{--} = \frac{\left(\varepsilon_{\mathrm{h2}}\kappa^{\mathrm{p2}}_{z,1} + \varepsilon_{\mathrm{h1}}\kappa^{\mathrm{p2}}_{z,2}\right)\left[(\varepsilon_{\mathrm{h2}} - \varepsilon_{\mathrm{h1}}) + \left(\kappa^{\mathrm{p1}}_{z,1} - \kappa^{\mathrm{p2}}_{z,2}\right)\left(\kappa^{\mathrm{p1}}_{z,1} + \kappa^{\mathrm{p2}}_{z,2}\right)\right]}{2\varepsilon_{\mathrm{h2}}\kappa^{\mathrm{p2}}_{z,1}\left(\kappa^{\mathrm{p1}}_{z,1} - \kappa^{\mathrm{p2}}_{z,1}\right)\left(\kappa^{\mathrm{p1}}_{z,1} + \kappa^{\mathrm{p2}}_{z,1}\right)}, \tag{A16}$$

$$t^{\mathrm{p11}}_{+-} = t^{\mathrm{p11}}_{-+} = \frac{\left(\varepsilon_{\mathrm{h2}}\kappa^{\mathrm{p1}}_{z,1} - \varepsilon_{\mathrm{h1}}\kappa^{\mathrm{p1}}_{z,2}\right)\left[(\varepsilon_{\mathrm{h2}} - \varepsilon_{\mathrm{h1}}) + \left(\kappa^{\mathrm{p1}}_{z,1} - \kappa^{\mathrm{p2}}_{z,2}\right)\left(\kappa^{\mathrm{p2}}_{z,1} + \kappa^{\mathrm{p1}}_{z,2}\right)\right]}{2\varepsilon_{\mathrm{h2}}\kappa^{\mathrm{p1}}_{z,1}\left(\kappa^{\mathrm{p1}}_{z,1} - \kappa^{\mathrm{p2}}_{z,1}\right)\left(\kappa^{\mathrm{p1}}_{z,1} + \kappa^{\mathrm{p2}}_{z,1}\right)}, \tag{A17}$$

$$t^{\mathrm{p12}}_{+-} = t^{\mathrm{p12}}_{-+} = \frac{\left(\varepsilon_{\mathrm{h2}}\kappa^{\mathrm{p1}}_{z,1} - \varepsilon_{\mathrm{h1}}\kappa^{\mathrm{p2}}_{z,2}\right)\left[(\varepsilon_{\mathrm{h2}} - \varepsilon_{\mathrm{h1}}) + \left(\kappa^{\mathrm{p2}}_{z,1} - \kappa^{\mathrm{p2}}_{z,2}\right)\left(\kappa^{\mathrm{p2}}_{z,1} + \kappa^{\mathrm{p2}}_{z,2}\right)\right]}{2\varepsilon_{\mathrm{h2}}\kappa^{\mathrm{p1}}_{z,1}\left(\kappa^{\mathrm{p1}}_{z,1} - \kappa^{\mathrm{p2}}_{z,1}\right)\left(\kappa^{\mathrm{p1}}_{z,1} + \kappa^{\mathrm{p2}}_{z,1}\right)}, \tag{A18}$$

$$t_{+-}^{\mathrm{p}21} = t_{-+}^{\mathrm{p}21} = \frac{\left(\varepsilon_{\mathrm{h}2}\kappa_{z,1}^{\mathrm{p}2} - \varepsilon_{\mathrm{h}1}\kappa_{z,2}^{\mathrm{p}1}\right)\left[\left(\varepsilon_{\mathrm{h}1} - \varepsilon_{\mathrm{h}2}\right) + \left(\kappa_{z,2}^{\mathrm{p}1} - \kappa_{z,1}^{\mathrm{p}1}\right)\left(\kappa_{z,2}^{\mathrm{p}1} + \kappa_{z,1}^{\mathrm{p}1}\right)\right]}{2\varepsilon_{\mathrm{h}2}\kappa_{z,1}^{\mathrm{p}2}\left(\kappa_{z,1}^{\mathrm{p}1} - \kappa_{z,1}^{\mathrm{p}2}\right)\left(\kappa_{z,1}^{\mathrm{p}1} + \kappa_{z,1}^{\mathrm{p}2}\right)}, \tag{A19}$$

$$t_{+-}^{\mathrm{p}22} = t_{-+}^{\mathrm{p}22} = \frac{\left(\varepsilon_{\mathrm{h}2}\kappa_{z,1}^{\mathrm{p}2} - \varepsilon_{\mathrm{h}1}\kappa_{z,2}^{\mathrm{p}2}\right)\left[\left(\varepsilon_{\mathrm{h}1} - \varepsilon_{\mathrm{h}2}\right) + \left(\kappa_{z,2}^{\mathrm{p}2} - \kappa_{z,1}^{\mathrm{p}1}\right)\left(\kappa_{z,2}^{\mathrm{p}2} + \kappa_{z,1}^{\mathrm{p}1}\right)\right]}{2\varepsilon_{\mathrm{h}2}\kappa_{z,1}^{\mathrm{p}2}\left(\kappa_{z,1}^{\mathrm{p}1} - \kappa_{z,1}^{\mathrm{p}2}\right)\left(\kappa_{z,1}^{\mathrm{p}1} + \kappa_{z,1}^{\mathrm{p}2}\right)}. \tag{A20}$$

The matrix $\mathcal{T}_{BC}$ is obtained analogously, with $m = 1$ for layer B and $m = 2$ for layer C.

The reflection operators $\hat{\rho}_1 = \hat{\rho}_2 = \hat{\rho}$ have the matrix representation similar to that of the transfer operators:

$$\hat{\rho} = \begin{pmatrix} r^{\mathrm{s}} & 0 & 0 \\ 0 & r^{\mathrm{p}11} & r^{\mathrm{p}12} \\ 0 & r^{\mathrm{p}21} & r^{\mathrm{p}22} \end{pmatrix}. \tag{A21}$$

The components of this matrix can be found by applying suitable boundary conditions at an interface of the nanorods and air. The complete set of these conditions consists of a pair of the standard boundary conditions (A5) and an additional physical condition that requires the current density to vanish at the ends of the nanorods: $J_z = 0$ [34,35]. It can be proven that this implies an ABC as in Eq. (A7). Indeed, when (A6) is applied to the field in the air region, it immediately results in a zero current; thus, (A7) enforces $J_z = 0$ on the side of the nanorods.

The wave field on the side of the nanorods is expressed as in (A9) and (A10), while the field on the air side is a superposition of S- and P-polarized waves propagating away from the interface (as above, without any loss of generality we let the interface be at $z = 0$ and consider the case where the air region is at $z > 0$):

$$\mathbf{E}_{\mathrm{t,a}} = (\hat{\mathbf{v}}, \kappa_{z,\mathrm{a}}\hat{\mathbf{u}}) \cdot e^{iz\hat{k}_{z,\mathrm{a}}} T, \tag{A22}$$

$$\eta_0 \mathbf{H}_{\mathrm{t,a}} = (-\kappa_{z,\mathrm{a}}\hat{\mathbf{u}}, \hat{\mathbf{v}}) \cdot e^{iz\hat{k}_{z,\mathrm{a}}} T, \tag{A23}$$

where $\hat{k}_{z,a} = [k_{z,\mathrm{a}},0;\ 0,k_{z,\mathrm{a}}]$ is a diagonal matrix with the z component of the propagation factor in air $k_{z,\mathrm{a}} = \sqrt{\omega^2\varepsilon_0\mu_0 - k_{\mathrm{t}}^2}$ on its main diagonal, $\kappa_{z,\mathrm{a}} = k_{z,\mathrm{a}}/(\omega\sqrt{\varepsilon_0\mu_0})$, and $T = (T^{\mathrm{s}}, T^{\mathrm{p}})^{\mathrm{T}}$ is a column vector of the complex amplitudes of the two waves propagating in the air region.

Inserting these expressions into the boundary conditions (A5)–(A7) and repeating the same procedure as for the interface of two layers of nanorods above, we obtain the following expressions for the reflection coefficients (A21):

$$r^{\mathrm{s}} = \frac{\kappa_z^{\mathrm{s}} - \kappa_{z,\mathrm{a}}}{\kappa_z^{\mathrm{s}} + \kappa_{z,\mathrm{a}}}, \tag{A24}$$

$$r^{\mathrm{p}11} = -\frac{\left(\kappa_z^{\mathrm{p}1} + \kappa_z^{\mathrm{p}2}\right)\left\{1 + \kappa_{z,\mathrm{a}}^2 - \kappa_z^{\mathrm{p}1}\kappa_z^{\mathrm{p}2} - \varepsilon_{\mathrm{h}}\left[1 + \kappa_{z,\mathrm{a}}\left(\kappa_z^{\mathrm{p}1} - \kappa_z^{\mathrm{p}2}\right)\right]\right\}}{\left(\kappa_z^{\mathrm{p}1} - \kappa_z^{\mathrm{p}2}\right)\left\{1 + \kappa_{z,\mathrm{a}}^2 + \kappa_z^{\mathrm{p}1}\kappa_z^{\mathrm{p}2} - \varepsilon_{\mathrm{h}}\left[1 - \kappa_{z,\mathrm{a}}\left(\kappa_z^{\mathrm{p}1} + \kappa_z^{\mathrm{p}2}\right)\right]\right\}}, \tag{A25}$$

$$r^{\mathrm{p}22} = \frac{\left(\kappa_z^{\mathrm{p}1} + \kappa_z^{\mathrm{p}2}\right)\left\{1 + \kappa_{z,\mathrm{a}}^2 - \kappa_z^{\mathrm{p}1}\kappa_z^{\mathrm{p}2} - \varepsilon_{\mathrm{h}}\left[1 - \kappa_{z,\mathrm{a}}\left(\kappa_z^{\mathrm{p}1} - \kappa_z^{\mathrm{p}2}\right)\right]\right\}}{\left(\kappa_z^{\mathrm{p}1} - \kappa_z^{\mathrm{p}2}\right)\left\{1 + \kappa_{z,\mathrm{a}}^2 + \kappa_z^{\mathrm{p}1}\kappa_z^{\mathrm{p}2} - \varepsilon_{\mathrm{h}}\left[1 - \kappa_{z,\mathrm{a}}\left(\kappa_z^{\mathrm{p}1} + \kappa_z^{\mathrm{p}2}\right)\right]\right\}}, \tag{A26}$$

$$r^{\mathrm{p}12} = -\frac{2\kappa_z^{\mathrm{p}2}\left(1 + \kappa_{z,\mathrm{a}}^2 - \left(\kappa_z^{\mathrm{p}2}\right)^2 - \varepsilon_{\mathrm{h}}\right)}{\left(\kappa_z^{\mathrm{p}1} - \kappa_z^{\mathrm{p}2}\right)\left\{1 + \kappa_{z,\mathrm{a}}^2 + \kappa_z^{\mathrm{p}1}\kappa_z^{\mathrm{p}2} - \varepsilon_{\mathrm{h}}\left[1 - \kappa_{z,\mathrm{a}}\left(\kappa_z^{\mathrm{p}1} + \kappa_z^{\mathrm{p}2}\right)\right]\right\}}, \tag{A27}$$

$$r^{\mathrm{p}21} = \frac{2\kappa_z^{\mathrm{p}1}\left(1 + \kappa_{z,\mathrm{a}}^2 - \left(\kappa_z^{\mathrm{p}1}\right)^2 - \varepsilon_{\mathrm{h}}\right)}{\left(\kappa_z^{\mathrm{p}1} - \kappa_z^{\mathrm{p}2}\right)\left\{1 + \kappa_{z,\mathrm{a}}^2 + \kappa_z^{\mathrm{p}1}\kappa_z^{\mathrm{p}2} - \varepsilon_{\mathrm{h}}\left[1 - \kappa_{z,\mathrm{a}}\left(\kappa_z^{\mathrm{p}1} + \kappa_z^{\mathrm{p}2}\right)\right]\right\}}. \tag{A28}$$

The expressions for $r^{\mathrm{p}mn}$ greatly simplify when the relative host permittivity on the side of nanorods is $\varepsilon_{\mathrm{h}} = 1$:

$$r^{\mathrm{p}11} = \frac{\left(\kappa_z^{\mathrm{p}1} - \kappa_{z,\mathrm{a}}\right)\left(\kappa_z^{\mathrm{p}1} + \kappa_z^{\mathrm{p}2}\right)}{\left(\kappa_z^{\mathrm{p}1} + \kappa_{z,\mathrm{a}}\right)\left(\kappa_z^{\mathrm{p}1} - \kappa_z^{\mathrm{p}2}\right)}, \tag{A29}$$

$$r^{\mathrm{p}22} = -\frac{\left(\kappa_z^{\mathrm{p}2} - \kappa_{z,\mathrm{a}}\right)\left(\kappa_z^{\mathrm{p}1} + \kappa_z^{\mathrm{p}2}\right)}{\left(\kappa_z^{\mathrm{p}2} + \kappa_{z,\mathrm{a}}\right)\left(\kappa_z^{\mathrm{p}1} - \kappa_z^{\mathrm{p}2}\right)}, \tag{A30}$$

$$r^{\mathrm{p}12} = \frac{2\kappa_z^{\mathrm{p}2}\left(\kappa_z^{\mathrm{p}2} - \kappa_{z,\mathrm{a}}\right)}{\left(\kappa_z^{\mathrm{p}1} + \kappa_{z,\mathrm{a}}\right)\left(\kappa_z^{\mathrm{p}1} - \kappa_z^{\mathrm{p}2}\right)}, \tag{A31}$$

$$r^{\mathrm{p}21} = -\frac{2\kappa_z^{\mathrm{p}1}\left(\kappa_z^{\mathrm{p}1} - \kappa_{z,\mathrm{a}}\right)}{\left(\kappa_z^{\mathrm{p}2} + \kappa_{z,\mathrm{a}}\right)\left(\kappa_z^{\mathrm{p}1} - \kappa_z^{\mathrm{p}2}\right)}. \tag{A32}$$

It is also seen that in this case the reflection coefficient for the S-polarized waves is $r^{\mathrm{s}} = 0$. This is because the S-polarized waves do not interact with thin wires; that is, these modes reflect only due to the dielectric permittivity contrast at the interface. Thus, in this situation, the S-polarized waves do not contribute to the Casimir force acting on the piston.

It is interesting that with the help of (A24)–(A28) it is possible to write down the eigenvalues of the operator $\hat{\rho}$ given

by (A21) in a closed form:

$$\lambda_1 = r^{\mathrm{s}}, \quad \lambda_2 = -\frac{1+\kappa_{z,\mathrm{a}}^2+\kappa_z^{\mathrm{p1}}\kappa_z^{\mathrm{p2}}-\varepsilon_{\mathrm{h}}\left[1+\kappa_{z,\mathrm{a}}\left(\kappa_z^{\mathrm{p1}}+\kappa_z^{\mathrm{p2}}\right)\right]}{1+\kappa_{z,\mathrm{a}}^2+\kappa_z^{\mathrm{p1}}\kappa_z^{\mathrm{p2}}-\varepsilon_{\mathrm{h}}\left[1-\kappa_{z,\mathrm{a}}\left(\kappa_z^{\mathrm{p1}}+\kappa_z^{\mathrm{p2}}\right)\right]}, \quad \lambda_3 = 1. \tag{A33}$$

When $\varepsilon_{\mathrm{h}} = 1$, the expression for λ_2 simplifies to

$$\lambda_2 = \frac{\left(\kappa_z^{\mathrm{p1}}-\kappa_{z,\mathrm{a}}\right)\left(\kappa_{z,\mathrm{a}}-\kappa_z^{\mathrm{p2}}\right)}{\left(\kappa_z^{\mathrm{p1}}+\kappa_{z,\mathrm{a}}\right)\left(\kappa_{z,\mathrm{a}}+\kappa_z^{\mathrm{p2}}\right)}, \tag{A34}$$

It can be verified that at the positive imaginary frequencies $\omega = i\xi$ the respective eigenvalues are such that $|\lambda_{1,2}| < 1$, as is seen from (9) and (A24) for λ_1, and from (10) and (A33) for λ_2, because the expression for λ_2 can be rewritten as $\lambda_2 = (A-B)/(A+B)$, where A and B are such that $A = \kappa_{z,\mathrm{a}}(\kappa_z^{\mathrm{p1}}+\kappa_z^{\mathrm{p2}}) > 0$, and $B = (1+\kappa_{z,\mathrm{a}}^2+\kappa_z^{\mathrm{p1}}\kappa_z^{\mathrm{p2}})/\varepsilon_{\mathrm{h}} - 1 > 2/\varepsilon_{\mathrm{h}} > 0$. When $\varepsilon_{\mathrm{h}} \geqslant 1$, it is possible to prove that $0 \leqslant \lambda_{1,2} < 1$.

In the main text, it was mentioned that the eigenvalues of the operator $\hat{\rho}e^{-2z\hat{\gamma}_z}$ determine the sign of the Casimir force. At $z = 0$, the eigenvalues of this operator are given by (A33). To study what happens at $z > 0$, we consider the important case when $\varepsilon_{\mathrm{h}} = 1$. As discussed above, in this case all eigenvalues of the reflection operator $\hat{\rho}$ are such that $0 \leqslant \lambda_{1,2,3} \leqslant 1$.

We denote the eigenvalues of the operator $\hat{\rho}e^{-2z\hat{\gamma}_z}$ as $\tilde{\lambda}_{1,2,3}$. Let us show that the eigenvalues $\tilde{\lambda}_{1,2,3}$ are all real and non-negative when $\varepsilon_{\mathrm{h}} = 1$. We introduce the attenuation factors $\gamma_{1,2,3}$ as follows: $\gamma_1 = -ik_z^{\mathrm{s}}$, $\gamma_{2,3} = -ik_z^{\mathrm{p1,2}}$ (they are real and positive at the positive imaginary frequencies $\omega = i\xi$). Now we notice that due to the special form (A21) of the operator $\hat{\rho}$, the first eigenvalue is $\tilde{\lambda}_1 = r^{\mathrm{s}}e^{-2z\gamma_1} = 0$. The remaining two eigenvalues $\tilde{\lambda}_{2,3}$ are the solutions of the quadratic equation

$$\tilde{\lambda}^2 - \tilde{\lambda}\mathrm{Tr} + \mathrm{Dt} = 0, \tag{A35}$$

where $\mathrm{Tr} = (x_1 r^{\mathrm{p11}} + x_2 r^{\mathrm{p22}})$ and $\mathrm{Dt} = x_1 x_2 (r^{\mathrm{p11}} r^{\mathrm{p22}} - r^{\mathrm{p12}} r^{\mathrm{p21}})$, $x_{1,2} = e^{-2z\gamma_{2,3}}$, are the trace and the determinant of the lower-right submatrix of $\hat{\rho}e^{-2z\hat{\gamma}_z}$ of rank 2, respectively. The discriminant of this equation is $\mathcal{D} = \mathrm{Tr}^2 - 4\mathrm{Dt} = (x_1 r^{\mathrm{p11}} - x_2 r^{\mathrm{p22}})^2 + 4x_1 x_2 r^{\mathrm{p12}} r^{\mathrm{p21}} \geqslant 0$, because $r^{\mathrm{p12}} r^{\mathrm{p21}} \geqslant 0$, as can be verified using Eqs. (10) and (A31)–(A32). Therefore, the eigenvalues $\tilde{\lambda}_{2,3}$ are real. It is also clear that they are non-negative, because $\mathrm{Dt} = x_1 x_2 \lambda_2 \lambda_3 \geqslant 0$ and $\sqrt{\mathcal{D}} \leqslant \mathrm{Tr}$.

[1] H. B. G. Casimir, Proc. K. Ned. Akad. Wet. **51**, 791 (1948).
[2] E. M. Lifshitz, Sov. Phys. JETP **2**, 73 (1956).
[3] I. E. Dzyaloshinski, E. M. Lifshitz, and L. P. Pitaevski, Adv. Phys. **10**, 165 (1965).
[4] T. H. Boyer, Phys. Rev. A **9**, 2078 (1974).
[5] O. Kenneth, I. Klich, A. Mann, and M. Revzen, Phys. Rev. Lett. **89**, 033001 (2002).
[6] E. Buks and M. L. Roukes, Nature (London) **419**, 119 (2002).
[7] C. Henkel and K. Joulain, Europhys. Lett. **72**, 929 (2005).
[8] I. G. Pirozhenko and A. Lambrecht, J. Phys. A: Math. Theor. **41**, 164015 (2008).
[9] A. W. Rodriguez, J. D. Joannopoulos, and S. G. Johnson, Phys. Rev. A **77**, 062107 (2008).
[10] F. S. S. Rosa, J. Phys.: Conf. Ser. **161**, 012039 (2009).
[11] U. Leonhardt and T. G. Philbin, New J. Phys. **9**, 254 (2007).
[12] M. Levin, A. P. McCauley, A. W. Rodriguez, M. T. H. Reid, and S. G. Johnson, Phys. Rev. Lett. **105**, 090403 (2010).
[13] A. W. Rodriguez, A. P. McCauley, D. Woolf, F. Capasso, J. D. Joannopoulos, and S. G. Johnson, Phys. Rev. Lett. **104**, 160402 (2010).
[14] S. J. Rahi and S. Zaheer, Phys. Rev. Lett. **104**, 070405 (2010).
[15] J. N. Munday, F. Capasso, and V. A. Parsegian, Nature (London) **457**, 170 (2009).
[16] R. M. Cavalcanti, Phys. Rev. D **69**, 065015 (2004).
[17] M. P. Hertzberg, R. L. Jaffe, M. Kardar, and A. Scardicchio, Phys. Rev. Lett. **95**, 250402 (2005).
[18] G. Barton, Phys. Rev. D **73**, 065018 (2006).
[19] A. Edery, Phys. Rev. D **75**, 105012 (2007).
[20] V. N. Marachevsky, J. Phys. A: Math. Theor. **41**, 164007 (2008).
[21] S. C. Lim and L. P. Teo, New J. Phys. **11**, 013055 (2009).
[22] E. Álvarez and F. D. Mazzitelli, Phys. Rev. D **79**, 045019 (2009).
[23] S. I. Maslovski and M. G. Silveirinha, Phys. Rev. A **82**, 022511 (2010).
[24] M. G. Silveirinha, Phys. Rev. B **82**, 085101 (2010).
[25] M. G. Silveirinha and S. I. Maslovski, Phys. Rev. A **82**, 052508 (2010).
[26] Z. Jacob, I. Smolyaninov, and E. Narimanov, e-print arXiv:0910.3981v2.
[27] Z. Jacob, J.-Y. Kim, G. Naik, A. Boltasseva, E. Narimanov, and V. Shalaev, Appl. Phys. B: Lasers Opt. **100**, 215 (2010).
[28] M. A. Noginov, H. Li, Y. A. Barnakov, D. Dryden, G. Nataraj, G. Zhu, C. E. Bonner, M. Mayy, Z. Jacob, and E. E. Narimanov, Opt. Lett. **35**, 1863 (2010).
[29] M. G. Silveirinha, Phys. Rev. E **73**, 046612 (2006).
[30] M. G. Silveirinha, P. A. Belov, and C. R. Simovski, Opt. Lett. **33**, 1726 (2008).
[31] S. I. Maslovski and M. G. Silveirinha, Phys. Rev. B **80**, 245101 (2009).
[32] N. V. Kampen, B. Nijboer, and K. Schram, Phys. Lett. A **26**, 307 (1968).
[33] A. Lambrecht and V. N. Marachevsky, J. Phys.: Conf. Ser. **161**, 012014 (2009).
[34] M. G. Silveirinha, IEEE Trans. Antennas Propag. **54**, 1766 (2006).
[35] M. G. Silveirinha, C. A. Fernandes, and J. R. Costa, New J. Phys. **10**, 053011 (2008).
[36] M. A. Ordal, R. J. Bell, J. R. W. Alexander, L. L. Long, and M. R. Querry, Appl. Opt. **24**, 4493 (1985).
[37] I. Brevik, J. B. Aarseth, J. S. Høye, and K. A. Milton, Phys. Rev. E **71**, 056101 (2005).
[38] S. J. Rahi, M. Kardar, and T. Emig, Phys. Rev. Lett. **105**, 070404 (2010).

[39] V. B. Bezerra, G. L. Klimchitskaya, V. M. Mostepanenko, and C. Romero, Phys. Rev. A **69**, 022119 (2004).

[40] V. B. Bezerra, R. S. Decca, E. Fischbach, B. Geyer, G. L. Klimchitskaya, D. E. Krause, D. López, V. M. Mostepanenko, and C. Romero, Phys. Rev. E **73**, 028101 (2006).

[41] J. S. Høye, I. Brevik, J. B. Aarseth, and K. A. Milton, J. Phys. A: Math. Gen. **39**, 6031 (2006).

[42] K. A. Milton, J. Phys.: Conf. Ser. **161**, 012001 (2009).

[43] R. K. Bansal, *A Textbook of Strength of Materials*, 4th ed. (Laxmi Publications, New Delhi, 2007).

[44] Z. M. Ao, S. Li, and Q. Jiang, Appl. Phys. Lett. **93**, 081905 (2008).

[45] G. Conache, S. M. Gray, A. Ribayrol, L. E. Froberg, L. Samuelson, L. Montelius, and H. Pettersson, J. Appl. Phys. **108**, 094307 (2010).

[46] G. Conache, S. M. Gray, A. Ribayrol, L. E. Fröberg, L. Samuelson, H. Pettersson, and L. Montelius, Small **5**(2), 203 (2009).

[47] M. Bordag, A. Ribayrol, G. Conache, L. Fröberg, S. Gray, L. Samuelson, L. Montelius, and H. Pettersson, Small **3**(8), 1398 (2007).

[48] D. A. R. Dalvit, F. C. Lombardo, F. D. Mazzitelli, and R. Onofrio, Phys. Rev. A **74**, 020101 (2006).

[49] S. I. Maslovski, T. A. Morgado, M. G. Silveirinha, C. S. R. Kaipa, and A. B. Yakovlev, New J. Phys. **12**, 113047 (2010).